Generalized-seniority pattern and thermal properties in even Sn isotopes

L. Y. Jia[1,*] and Chong Qi[2]

[1]*Department of Physics, University of Shanghai for Science and Technology, 200093 Shanghai, People's Republic of China*

[2]*Department of Physics, Royal Institute of Technology (KTH), SE-10691 Stockholm, Sweden*

(Received 8 May 2016; revised manuscript received 28 August 2016; published 17 October 2016)

Even tin isotopes of mass number $A = 108$–124 are calculated with realistic interactions in the generalized-seniority approximation of the nuclear shell model. For each nucleus, we compute the lowest 10 000 states (5000 of each parity) up to around 8 MeV in excitation energy, by allowing as many as four broken pairs. The lowest 50 eigen energies of each parity are compared with the exact results of the large-scale shell-model calculation. The wave functions of the midshell nuclei show a clear pattern of the stepwise breakup of condensed coherent pairs with increasing excitation energy. We also compute in the canonical ensemble the thermal properties—level density, entropy, and specific heat—in relation to the thermal pairing phase transition.

DOI: 10.1103/PhysRevC.94.044312

I. INTRODUCTION

The similarity between metal superconductivity and nuclear superfluidity was soon recognized [1,2] after the highly successful BCS theory [3]. In the superconducting ground state, electrons are coupled into pairs by the lattice-mediated effective attraction. In nuclei the short-range pairing force tends to couple nucleons. Although the pairing force influences practically all nuclei across the nuclear chart, the best superfluids are found among spherical semimagic and near-magic nuclei. In these nuclei, the pairing force dominates over other correlations, including the most important quadrupole-quadrupole one. As a result, the ground state is largely a condensate of coherent pairs, well separated from the rest states by the pairing gap.

Naturally, we would ask to what extent this superfluid structure persists at higher energies in the increasingly dense spectrum. In a purely pairing model, the states with s broken pairs are roughly degenerate at s times the pairing gap. But in reality other correlations may disturb this picture.

In the standard BCS and Bogoliubov quasiparticle formalism, one may consider diagonalizing $\hat{H} - \lambda\hat{N}$ (λ is the chemical potential) in the subspaces with two or more quasiparticles until convergence. However, the eigen wave functions—even for the lowest states—usually have a large number of quasiparticles and thus converge slowly (see Sec. 2.3.3. of Ref. [4] and references therein). This is due to the particle-number violating nature of the quasiparticle formalism. Instead the most natural approach seems to be the generalized-seniority truncation of the shell model. The starting point is the fully paired state [Eq. (3) below] that is the trial BCS wave function projected onto the good particle number. The coherent pair structure is usually fixed by minimizing the mean energy in the variation principle. As a truncation scheme of the shell model, we break the coherent pairs and diagonalize the Hamiltonian H in the subspace consisting of all the states with $S = 2s$ unpaired nucleons. [The subspace of S unpaired nucleons consists of the subspaces of generalized-seniority $S, S-2, \ldots, 2, 0$; see Eq. (6).] With increasing S and thus the subspace size, the eigen wave functions gradually converge to the exact shell-model ones when all the pairs are broken. The distribution in terms of generalized seniority is given by the amplitudes of various S components in the eigen wave function.

The long chain of tin isotopes is a classic example of nuclear superfluidity and attracts continuous attention. Recent theoretical investigations include, for example, the mean-field theory [5–10], the nuclear shell model [11–14], and the schematic generalized-seniority description [15–17]. The near constancy of the first 2^+ excitation energy suggests strong pairing correlations and led Talmi [15,18,19] to propose the generalized seniority as a good quantum number of the Hamiltonian. Realistic Hamiltonians may not satisfy the derived restrictions, and the universal method should be the diagonalization of the Hamiltonian in the subspace of S unpaired nucleons (the subspace up to generalized-seniority S). This has been done in the neutron 50–82 major shell with either phenomenological or more realistic interactions for $S = 2$ [20,21] and $S = 4$ [4,22], but with modern realistic interactions [23] only for $S = 2$ [11,24]. However, as pointed out in these works, higher S is necessary to achieve convergence, which is challenging and not done yet. Using the fast algorithm for generalized seniority we developed [25] and applied [26] recently, in this work we compute with modern realistic interactions [13] the lowest 10 000 states (5000 of each parity) of $^{108-124}$Sn in the subspace of $S = 8$ unpaired nucleons (up to generalized-seniority $S = 8$). The distribution of wave functions in terms of generalized seniority is examined in detail. The results show that the superfluid structure indeed persists in the higher dense spectrum, and the picture of the successive breakup of coherent pairs is approximately valid, especially so near the midshell.

The thermal properties of tin isotopes related to the pairing phase transition have been the subject of many recent studies. The level densities up to the neutron separation energy in ^{116,118,122}Sn have been extracted experimentally under certain assumptions [27–29], together with the specific heat and entropy. Theoretically, the thermal properties could be computed by the finite-temperature mean-field theory [10,30,31].

*liyuan.jia@usst.edu.cn

When practical, the spectroscopically accurate shell-model-type approaches are possibly more accurate. The shell-model Monte Carlo method [32,33] is suitable by its formulation to compute canonical-ensemble properties, but is limited by the sign problem. Successful applications [34–41] must use the good-sign Hamiltonian extracted from the full realistic interaction. The standard shell model is able to compute couples of the low-lying states but is still time-consuming near the midshell [13]. Accurate thermal properties in the canonical ensemble require usually thousands of states and few calculations have been done in this way [42]. In this work we are able to compute the lowest 10 000 states owing to the relatively small dimension of the generalized-seniority truncated subspace ($S = 8$), from which the canonical-ensemble quantities at low temperature are calculated. The transition from the superfluid phase to the normal phase is reproduced.

Section II briefly reviews the generalized-seniority formalism. The results for tin isotopes are presented in Sec. III inspecting the generalized-seniority structure of the eigen wave functions. Based on the spectrum, we compute canonical-ensemble thermal properties in Sec. IV in relation to the pairing phase transition. Section V summarizes the work.

II. GENERALIZED SENIORITY FORMALISM

We briefly review the generalized-seniority formalism in relation to the current work. The pair-creation operator

$$P_\alpha^\dagger = a_\alpha^\dagger a_{\tilde{\alpha}}^\dagger \tag{1}$$

creates a pair of particles on the single-particle level $|\alpha\rangle$ and its time-reversed partner $|\tilde{\alpha}\rangle$ ($|\tilde{\tilde{\alpha}}\rangle = -|\alpha\rangle, P_\alpha^\dagger = P_{\tilde{\alpha}}^\dagger$). The coherent pair-creation operator

$$P^\dagger = \sum_{m_\alpha > 0} v_\alpha P_\alpha^\dagger \tag{2}$$

creates a pair of particles coherently distributed with structure coefficients v_α over the entire single-particle space, where the summation runs over orbits with a positive magnetic quantum number m_α. The pair-condensate wave function of the $2N$-particle system

$$(P^\dagger)^N |\text{vac}\rangle \tag{3}$$

builds in pairing correlations, where $|\text{vac}\rangle$ is the vacuum state.

Gradually breaking coherent pairs, the state with $S = 2s$ unpaired nucleons is

$$\underbrace{a^\dagger a^\dagger \dots a^\dagger}_{S=2s} (P^\dagger)^{N-s} |0\rangle. \tag{4}$$

Loosely speaking, S is defined as the generalized-seniority quantum number [4,18,19,21,43,44]. More precisely, we distinguish between the space $|S\}$ of S unpaired nucleons and the space $|S\rangle$ of generalized-seniority S. The space $|S\}$ consists of all the states of the form (4). Any state of $S' < S$ unpaired nucleons can be written as a linear combination of the states of S unpaired nucleons, after substituting several $P^\dagger$ by Eq. (2). Therefore $|S'\}$ is a subspace of $|S\}$,

$$|S\} \supset |S-2\} \supset |S-4\} \supset \cdots \supset |2\} \supset |0\}. \tag{5}$$

In contrast, $|S\rangle$ is the subspace after removing the subspace $|S-2\}$ from the space $|S\}$, thus

$$\begin{aligned} |S\} &= |S\rangle \cup |S-2\} \\ &= |S\rangle \cup |S-2\rangle \cup |S-4\} \\ &= \cdots \\ &= |S\rangle \cup |S-2\rangle \cup \cdots \cup |2\rangle \cup |0\rangle. \end{aligned} \tag{6}$$

The symbol "∪" means set union. In this work $S = 2s$ is even, and we define $|s\} \equiv |S\}$ and $|s\rangle \equiv |S\rangle$. The original basis vectors (4) are not orthogonal. After orthonormalization the new basis vectors of the space $|s\rangle$ are enumerated as $|s,i\rangle$, where the index i runs from one to the dimension of $|s\rangle$.

Practical generalized-seniority calculations usually truncate the full many-body space to the subspace $|s\}$ and then diagonalize the Hamiltonian ($s = N$ corresponds to the full space without truncation). The eigen wave function is

$$|E\rangle = \sum_{s' \leqslant s} \sum_i c_{s',i} |s',i\rangle. \tag{7}$$

Investigating the wave function (7) in terms of generalized seniority, the amplitude for generalized-seniority $2s'$ is

$$P(s') = \sum_i |c_{s',i}|^2, \tag{8}$$

and $\sum_{s' \leqslant s} P(s') = 1$. The average of s is

$$\bar{s} = \sum_{s' \leqslant s} s' P(s'). \tag{9}$$

The average of s^2 is

$$\overline{s^2} = \sum_{s' \leqslant s} (s')^2 P(s'). \tag{10}$$

The fluctuation of s is

$$\Delta s = \sqrt{\overline{(s-\bar{s})^2}} = \sqrt{\overline{s^2} - (\bar{s})^2}. \tag{11}$$

III. GENERALIZED-SENIORITY PATTERN

In this work even tin isotopes of mass number $A = 108$–124 are computed in the generalized-seniority truncation of the shell model to four broken pairs (up to generalized-seniority eight). The doubly magic $^{100}_{50}$Sn is taken as an inert core and the valence neutrons distribute in the 50–82 major shell. We take the Hamiltonian from Ref. [13]. It starts from the realistic CD-Bonn nucleon-nucleon potential [45] and is renormalized in the perturbative G-matrix approach [23]. Then the monopole terms and unknown single-particle energies are fitted [13] to the 157 experimental low-lying yrast energies in $^{102-132}$Sn of both even and odd masses. This Hamiltonian has been used in Refs. [46–51].

The coherent pair structure $v_j = v_{jm}$ (2) is independent of the magnetic quantum number m because of the rotational symmetry. For each nucleus we determine v_j in the variation principle through minimizing the mean energy of the fully paired state [Eq. (3), $S = 0$]. This state has the particle-hole symmetry [52]; the energy minimum and the wave function (3) are independent of choosing the particles or the holes as the

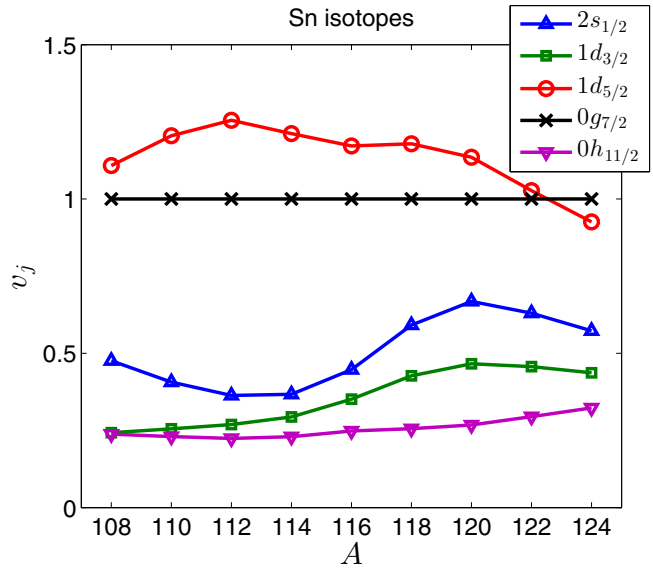

FIG. 1. Collective pair structures v_j (2) in tin isotopes (A is the mass number). They are normalized such that $v_{0g_{7/2}} = 1$.

degree of freedom. The particle-pair structures and the hole-pair structures are reciprocals of each other [$v_j^{\text{hole}} = 1/v_j^{\text{particle}}$ in Eq. (2)]. Figure 1 shows the particle-pair structures v_j^{particle} in $^{108-124}$Sn normalized by setting $v_{0g_{7/2}}^{\text{particle}} = 1$. In the isotopic chain v_j's vary smoothly with the mass number. The two orbits $0g_{7/2}$ and $1d_{5/2}$ that are lower in energy have larger v_j and bigger occupancy.

In this work we truncate the full shell-model space to the subspace of four broken pairs $|s = 4\}$ [the subspace up to generalized-seniority $S = 2s = 8$, see Eq. (6)]. The Hamiltonian matrix in the M scheme has the dimension 646 430 (for $M = 0$ including both parities). The basis (4) of the space $|s = 4\}$ is in general not orthogonal, and the nontrivial overlap matrix of the basis has the same dimension. By the recent fast algorithm of generalized seniority [25], we compute the Hamiltonian and the overlap matrices that are both *sparse*. The generalized (nonorthogonal basis) eigenvalue problem is solved by the MATLAB function "eigs" in the Lanczos method for the lowest 5000 eigenstates of each parity. In Ref. [53] we proved that the truncation up to an arbitrary generalized seniority preserves the particle-hole symmetry; the particle $|s\}$ and the hole $|s\}$ are the same subspace [$0 \leqslant s \leqslant \min(N, \Omega - N)$, where $2\Omega = \sum_j (2j + 1)$]. At a given nucleus the results are independent of choosing the particles or the holes as the degree of freedom. Practically we calculate $^{108-116}$Sn in the particle representation and $^{118-124}$Sn in the hole representation. The results for ^{108}Sn and ^{124}Sn are the exact shell-model ones because all the pairs (of particles or holes) are broken; others are approximations.

To evaluate the quality of the approximation, we perform large-scale shell-model calculations for the lowest 50 eigenstates of each parity in $^{110-122}$Sn. Figures 2 and 3 show the errors dE of the generalized-seniority eigenenergies, relative to the exact shell-model ones. The errors dE are computed assuming that the J_i^P generalized-seniority eigenstate corresponds to the J_i^P shell-model eigenstate (J_i^P stands for the ith lowest eigenstate of angular momentum J and parity P). We introduce the symbol $E_{s=1}^<$ as the energy below which the number of many-body eigenstates is equal to the dimension of the $|s = 1\}$ subspace (6). ($E_{s=1}^<$ is somehow similar to the concept of the Debye frequency of a crystal.) The vertical dotted line on each panel represents $E = E_{s=1}^<$; to the left of this line the number of data points is equal to the dimension of the $|s = 1\}$ subspace (6). We see in Fig. 2 that the ground-state energies converge very well. The actual numbers are $dE = 3$, 4, 7, 10, 9, 7, and 3 keV for $^{110-122}$Sn. Below $E_{s=1}^<$, the errors from Figs. 2 and 3 are generally small, running from around 10 keV to about 100 keV, except for ^{118}Sn and ^{120}Sn where the errors are around 200 keV near $E_{s=1}^<$. In most cases the

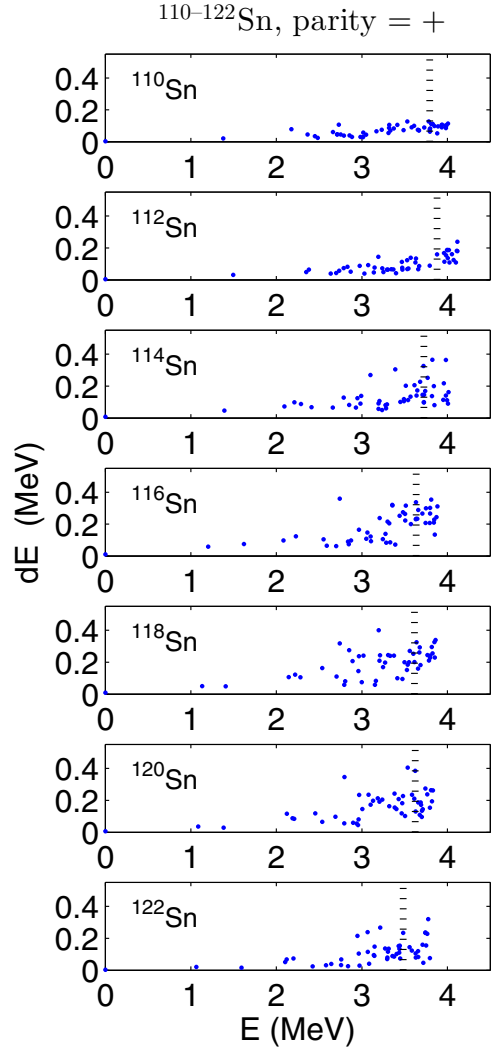

FIG. 2. Errors of the generalized-seniority eigen energies for the lowest 50 positive-parity eigenstates in $^{110-122}$Sn. Every panel has 50 data points, each represents one J state. The horizontal coordinate is the exact excitation energy from the shell-model calculation. The vertical coordinate is the error of the eigenenergy from the generalized-seniority calculation, relative to the exact shell-model eigenenergy. The vertical dotted line is $E = E_{s=1}^<$ as explained in the text.

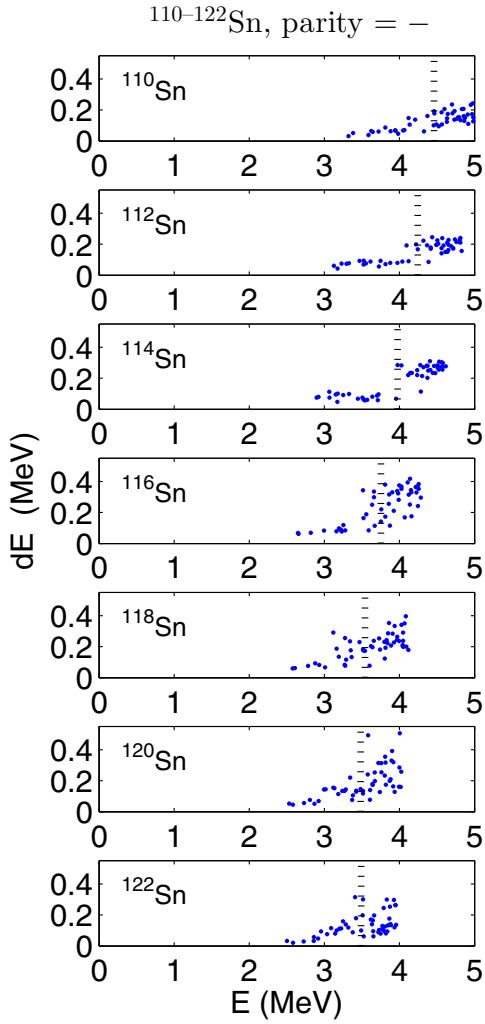

FIG. 3. Errors of the generalized-seniority eigenenergies for the lowest 50 negative-parity eigenstates in $^{110-122}$Sn.

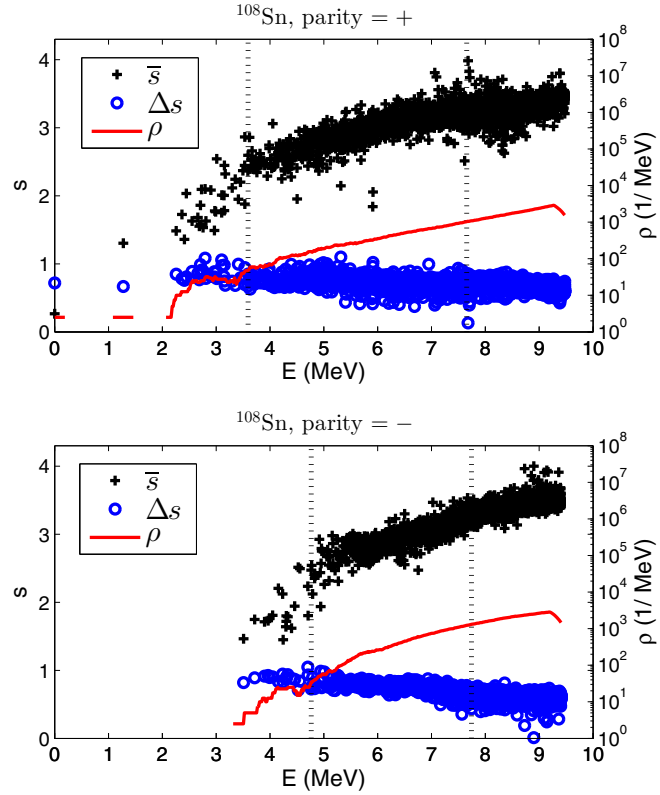

FIG. 4. The generalized-seniority ($S = 2s$) mean $\bar{s}$ and fluctuation Δs, and the level density ρ, versus the excitation energy in ^{108}Sn. The upper (lower) panel plots the lowest 5000 eigenstates with positive (negative) parity. Each black plus (blue circle) symbol represents one state; its horizontal coordinate is the excitation energy, and the vertical coordinate is $\bar{s}$ (Δs) corresponding to the left axis. The red solid line corresponding to the right axis plots the level density ρ averaged over an energy bin of 0.4 MeV. The two vertical dotted lines are $E = E^{<}_{s=1}$ and $E = E^{<}_{s=2}$, respectively.

errors have a sudden increase beyond $E^{<}_{s=1}$, to 200–350 keV. This is related to the breakup of the second condensed pair as is shown in Figs. 4–21. The convergence for higher excited states by the generalized-seniority calculation are demonstrated later in another way when discussing Figs. 13–21.

For each eigen wave function, we compute its generalized-seniority amplitudes $P(s)$ (8), mean $\bar{s}$ (9), and fluctuation Δs (11). The results of $\bar{s}$ and Δs are plotted in Figs. 4–12, together with the level density

$$\rho(E) \equiv \frac{\Omega(E - dE, E + dE)}{2dE}, \tag{12}$$

where $\Omega(E - dE, E + dE)$ is the number of J levels in the energy interval $(E - dE, E + dE)$, and $dE = 0.2$ MeV. [$\rho(E)$ does not include the magnetic degeneracies.] The drop of the $\rho(E)$ curves at the large-energy end is artificial and simply because the maximal energy (the energy of the 5000th eigenstate) is reached, beyond which the J levels are not computed, thus absent from Eq. (12).

Intuitively, from pure pairing models we would expect a relatively sharp staircase curve of $\bar{s}$; breaking each pair costs roughly the pairing energy 2Δ (in BCS language). Realistic nuclei have generalized-seniority mixing interactions, and we would like to see to what extent they disturb the staircase pattern of $\bar{s}$. Figures 4–12 show the $\bar{s}$ curves for the tin isotopes $^{108-124}$Sn. The two vertical dotted lines on each figure represent $E = E^{<}_{s=1}$ and $E = E^{<}_{s=2}$; to the left of the first (second) line the number of data points is equal to the dimension of the $\{s = 1\}$ ($\{s = 2\}$) subspace (6). We see that the staircase pattern of $\bar{s}$ is more identifiable (less disturbed) near the midshell and for negative-parity states. The negative-parity stair at $E^{<}_{s=1}$ is obvious in $^{110-118}$Sn; the positive-parity stair at $E^{<}_{s=1}$ is identifiable in $^{112-116}$Sn. The stairs at $E^{<}_{s=2}$ are difficult to identify and, in $^{112-118}$Sn only, there are some relics for both parities.

The fact that the $\bar{s}$ staircase pattern is more identifiable near the midshell seems consistent with the conventional wisdom that the collective pairing effect is proportional to $N(\Omega - N)$. The factor $N(\Omega - N)$ appears in the expression of $B(E2; 2^+_1 \to 0^+_1)$ in the degenerate-seniority model [19]. This factor also appears in Belyaev's estimation of the BCS critical pairing strength under certain assumptions [2]. Usually

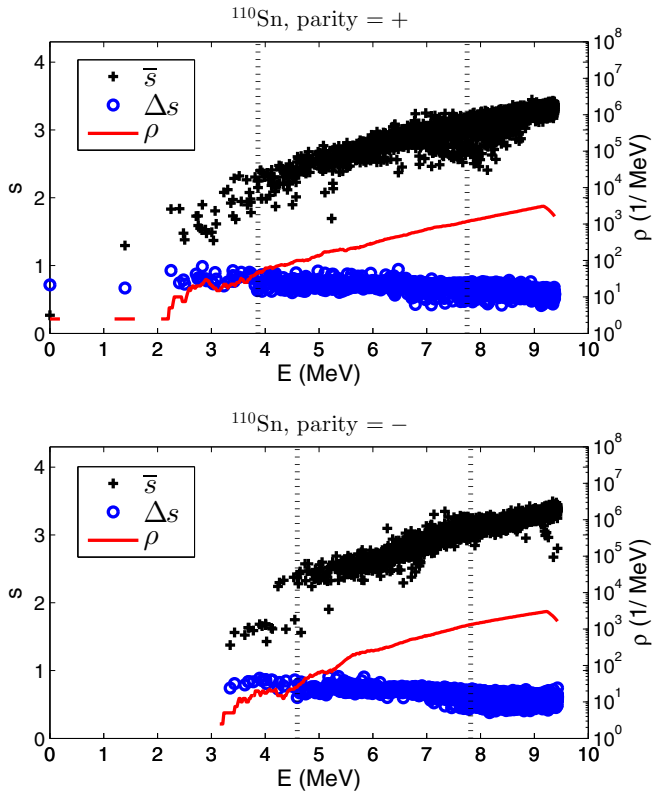

FIG. 5. The generalized-seniority mean and fluctuation, and the level density, versus the excitation energy in ^{110}Sn.

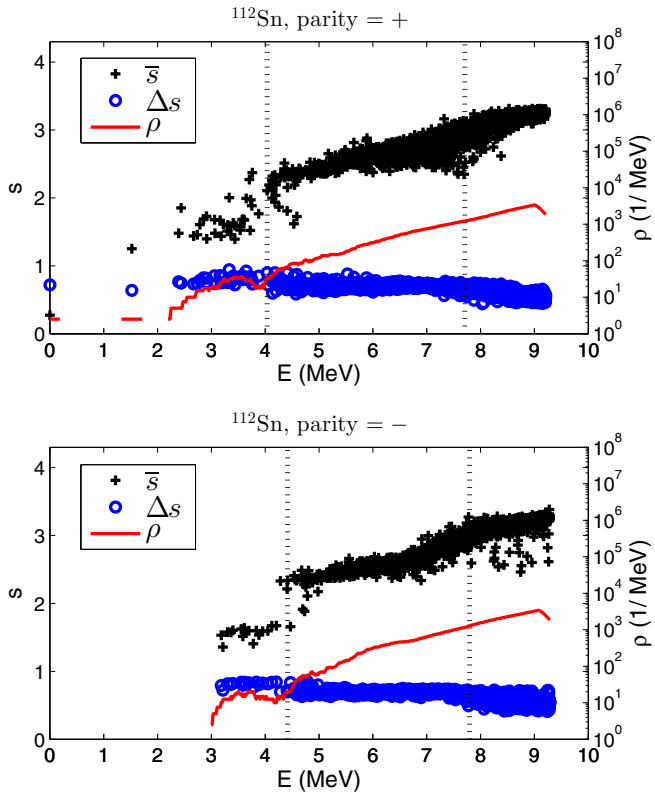

FIG. 6. The generalized-seniority mean and fluctuation, and the level density, versus the excitation energy in ^{112}Sn.

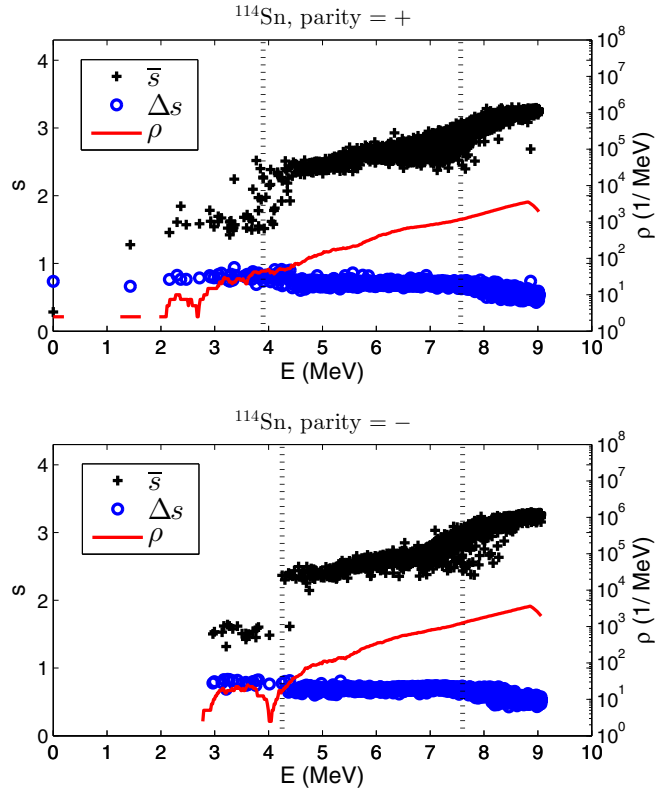

FIG. 7. The generalized-seniority mean and fluctuation, and the level density, versus the excitation energy in ^{114}Sn.

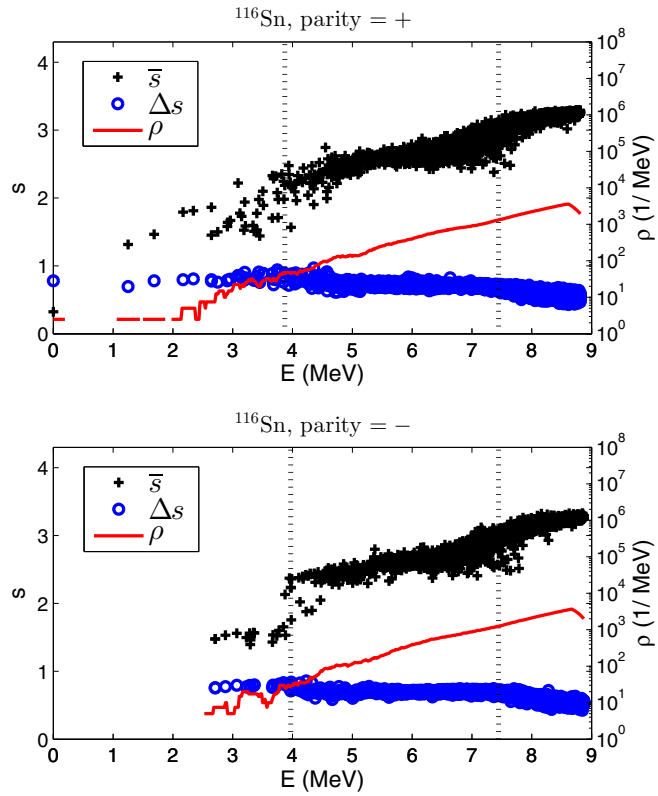

FIG. 8. The generalized-seniority mean and fluctuation, and the level density, versus the excitation energy in ^{116}Sn.

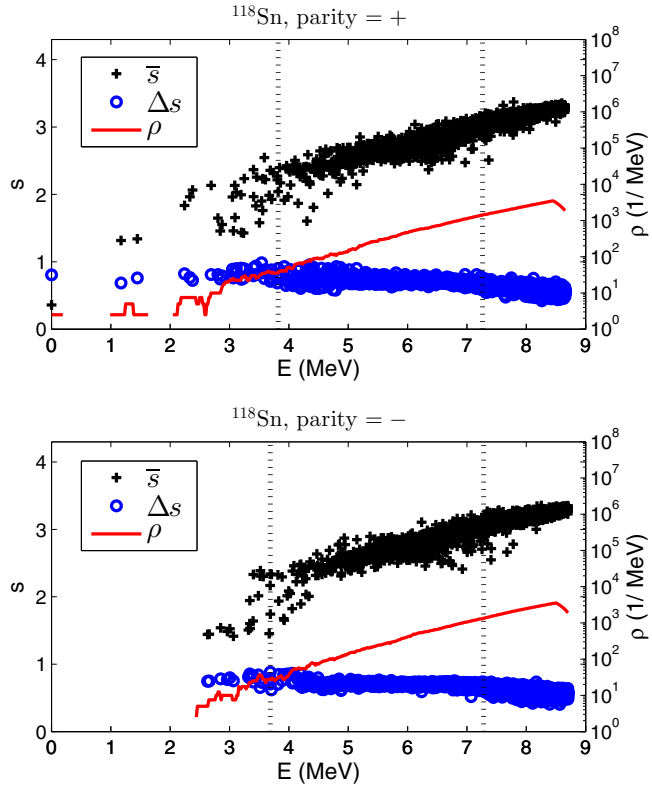

FIG. 9. The generalized-seniority mean and fluctuation, and the level density, versus the excitation energy in ^{118}Sn.

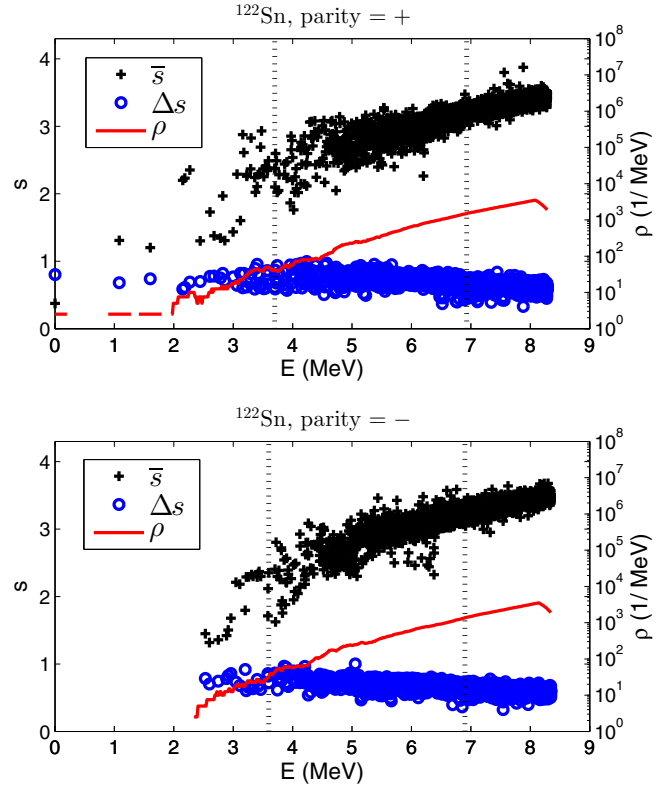

FIG. 11. The generalized-seniority mean and fluctuation, and the level density, versus the excitation energy in ^{122}Sn.

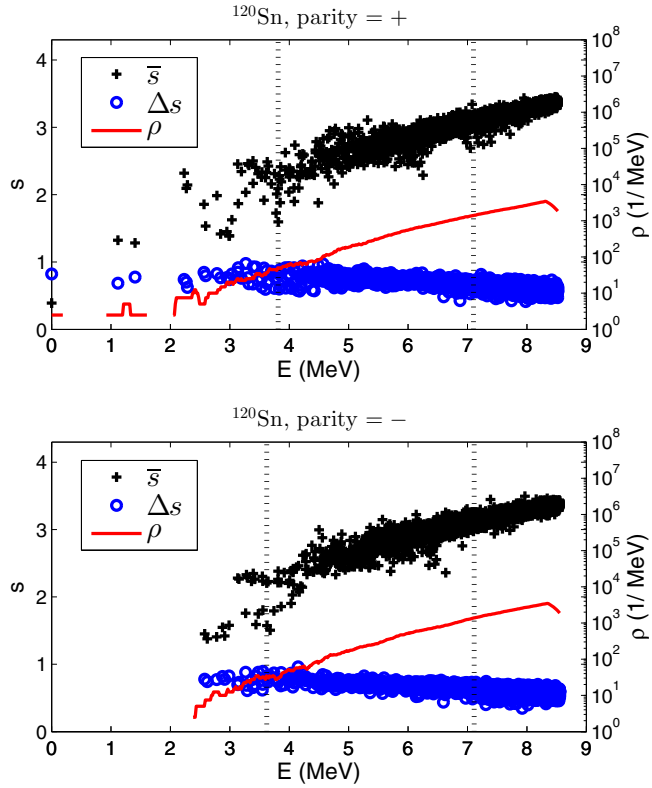

FIG. 10. The generalized-seniority mean and fluctuation, and the level density, versus the excitation energy in ^{120}Sn.

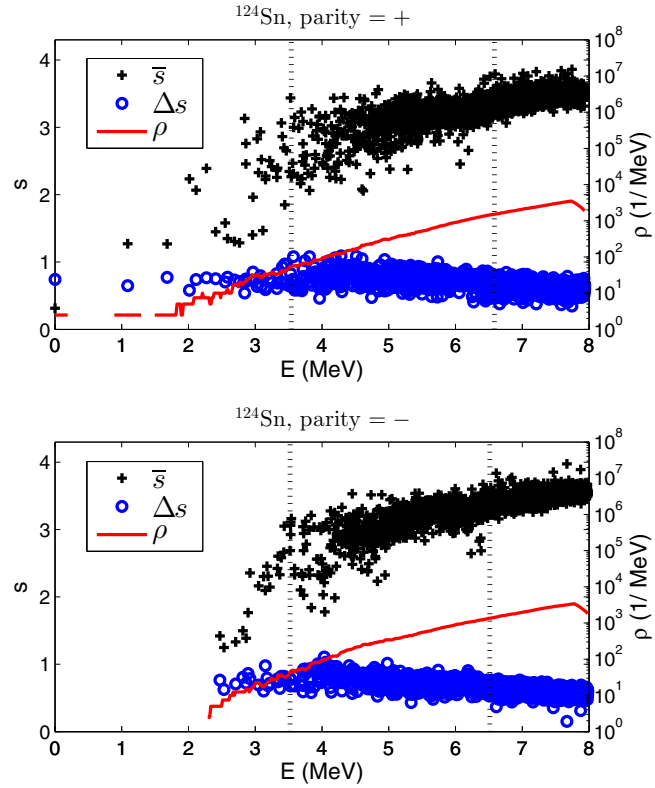

FIG. 12. The generalized-seniority mean and fluctuation, and the level density, versus the excitation energy in ^{124}Sn.

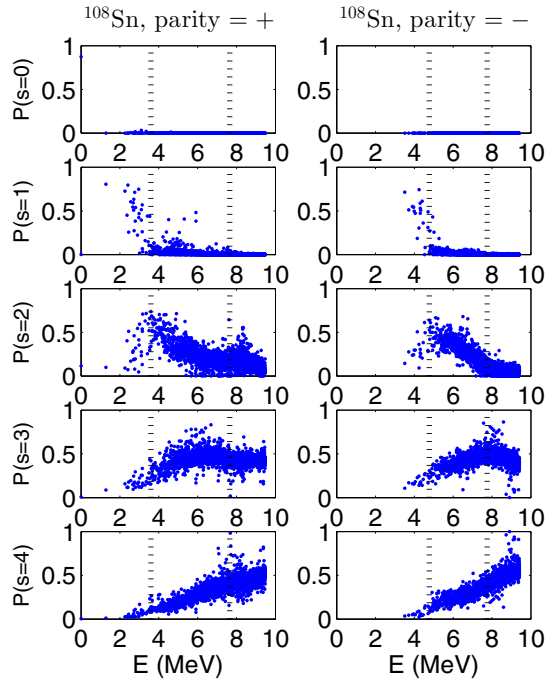

FIG. 13. Amplitudes $P(s)$ of each generalized seniority $S = 2s$ versus the excitation energy in ^{108}Sn. The left (right) panels plot the lowest 5000 eigenstates with positive (negative) parity. Therefore each panel has 5000 data points. The two vertical dotted lines $E = E^{<}_{s=1}$ and $E = E^{<}_{s=2}$ are at the same positions as those in Fig. 4.

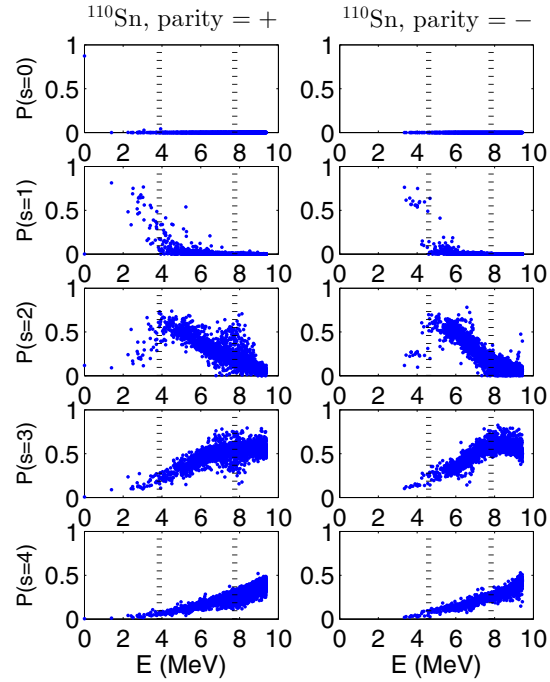

FIG. 14. Amplitudes of each generalized seniority versus the excitation energy in ^{110}Sn.

the midshell region has the largest effective model space ($\Omega_{\rm eff}$) available for the collective pairing; the Fermi surface sits in the middle and both upper and lower single-particle levels participate. This region also has the largest number of pairs $N \lesssim \Omega/2$ (particle and hole representations in the lower and upper shell, respectively). Therefore near the midshell the collective pairing effect is the most enhanced and the pair condensate seems the best developed. As a signature the staircase pattern is the most identifiable in Figs. 6–9 for $^{112\sim118}$Sn. We see that the jumps of the $\bar{s}$ curves happen roughly at $E = E^{<}_{s}$, especially so for $s = 1$. In this sense the generalized-seniority truncation gives the full low-lying spectrum around the midshell and no further dimension reduction is possible. $E^{<}_{s=2}$ is slightly below twice $E^{<}_{s=1}$. It is consistent with the degenerate-seniority model where this ratio is $2(1 - 1/\Omega)$. If we take $\Omega = 16$ (for the 50–82 major shell), this ratio is 1.875, quite consistent with those in Figs. 6–9 for $^{112-118}$Sn.

On the other hand, Figs. 4, 11, and 12 show that away from the midshell the staircase pattern is difficult to identify in ^{108,122,124}Sn. Here the available effective model space $\Omega_{\rm eff}$ is relatively small. The pair condensate does not seem well developed with the limited number of collective pairs. Other correlations may easily destroy the staircase pattern at higher energies.

Looking more closely, ^{114}Sn has the most clear stairs at $E = E^{<}_{s=1}$ instead of the exact midshell nucleus ^{116}Sn. This may indicate slightly reduced collective pairing at ^{116}Sn and seems consistent with the trend of the experimental $B(E2; 2^{+}_{1} \rightarrow 0^{+}_{1})$ values [54–57]. The $B(E2)$ values have a small dip at ^{116}Sn in the generally parabolic [proportional to $N(\Omega - N)$ in the degenerate-seniority model] curve for tin isotopes. This phenomenon has been explained in Ref. [15] by the different filling rates of the two groups of j orbits as follows. The

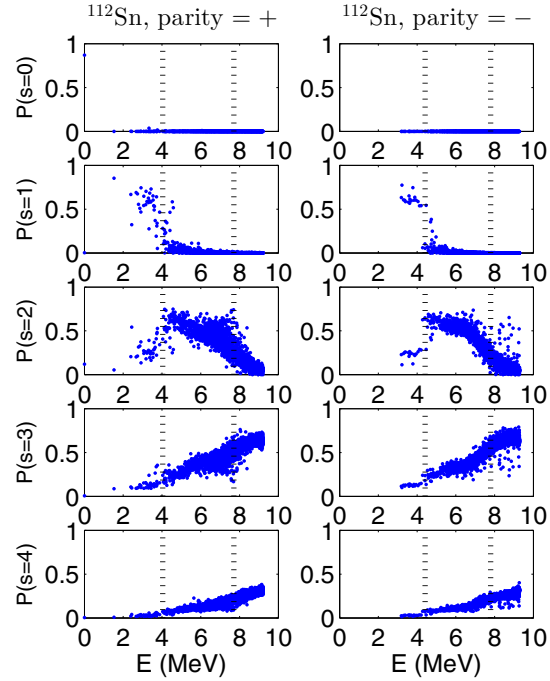

FIG. 15. Amplitudes of each generalized seniority versus the excitation energy in ^{112}Sn.

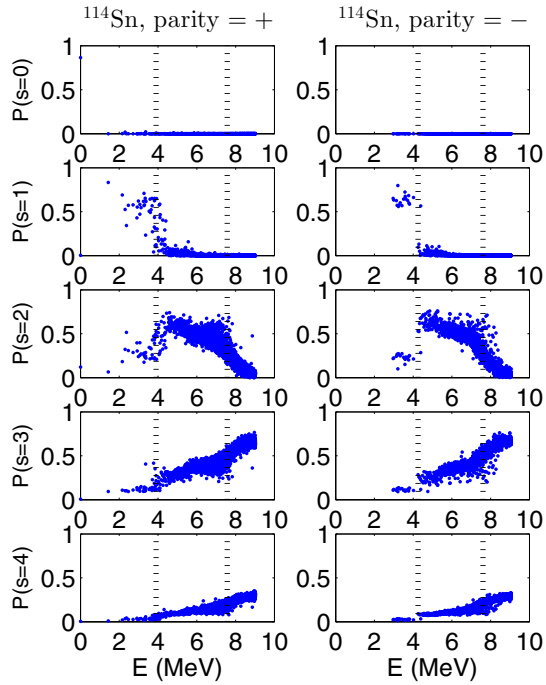

FIG. 16. Amplitudes of each generalized seniority versus the excitation energy in ^{114}Sn.

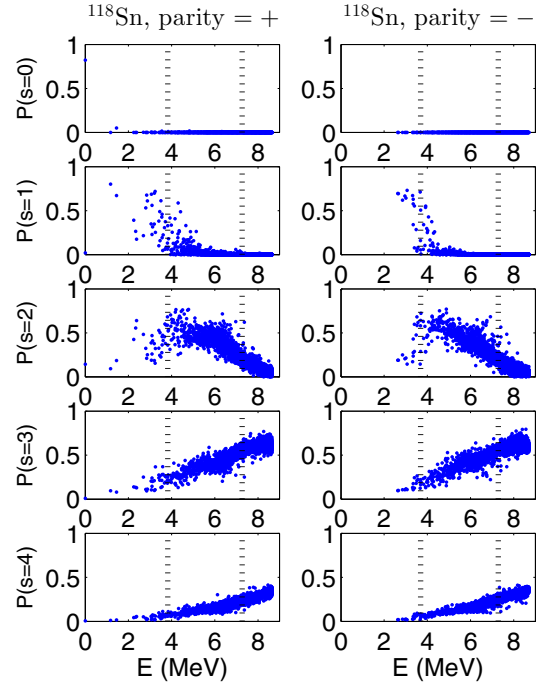

FIG. 18. Amplitudes of each generalized seniority versus the excitation energy in ^{118}Sn.

lower group has two orbits, $0g_{7/2}$ and $1d_{5/2}$, and the higher group has three orbits, $2s_{1/2}$, $1d_{3/2}$, and $0h_{11/2}$. The two groups are separated by a moderate energy difference. In the lower (upper) shell mainly the lower (higher) group contributes to the coherent pairing. At ^{116}Sn the occupation switches between the two groups and results in slightly reduced collective pairing.

Another observation is that the staircase pattern is more obvious for negative-parity states than for positive-parity states. This is likely related to the intruder orbit $0h_{11/2}$. It might

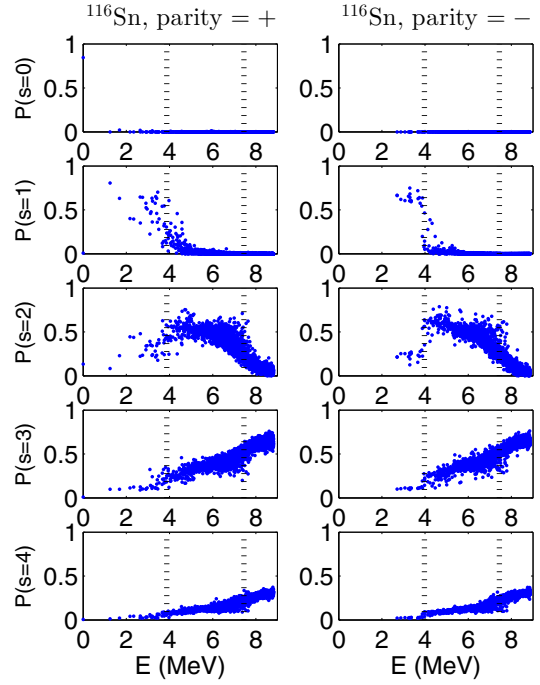

FIG. 17. Amplitudes of each generalized seniority versus the excitation energy in ^{116}Sn.

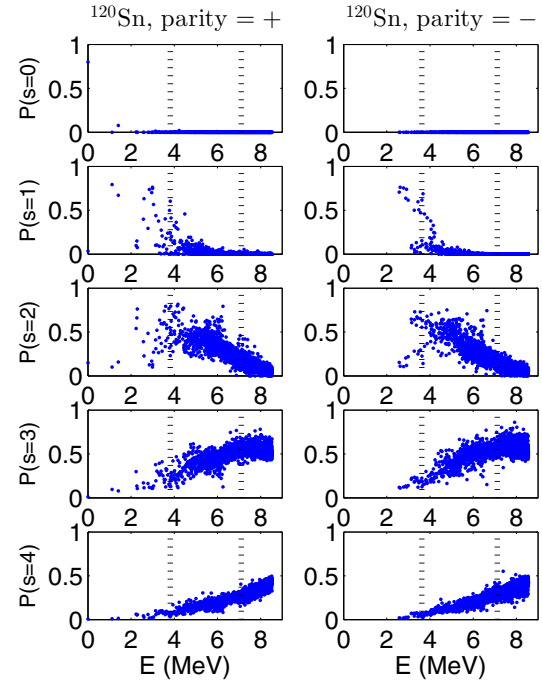

FIG. 19. Amplitudes of each generalized seniority versus the excitation energy in ^{120}Sn.

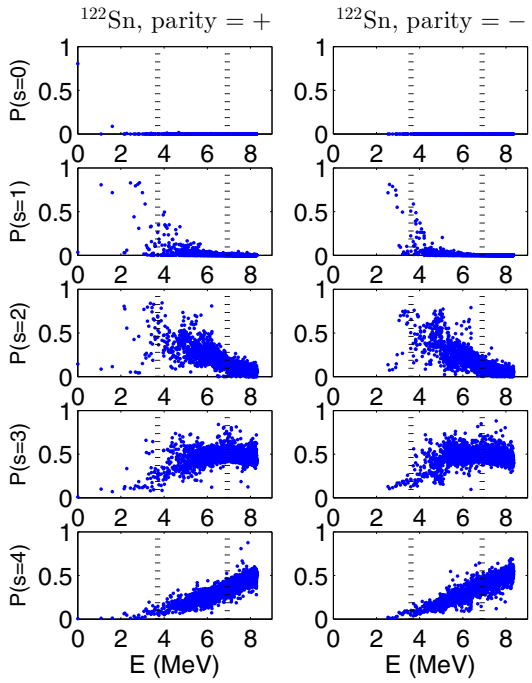

FIG. 20. Amplitudes of each generalized seniority versus the excitation energy in ^{122}Sn.

be due to the Hamiltonian two-body matrix elements involving $0h_{11/2}$ or to the smaller dimension of the negative-parity $|s = 1\}$ subspace (compared with that of the positive parity). It would be interesting to see whether this observation is true in other nuclei and to study its origin.

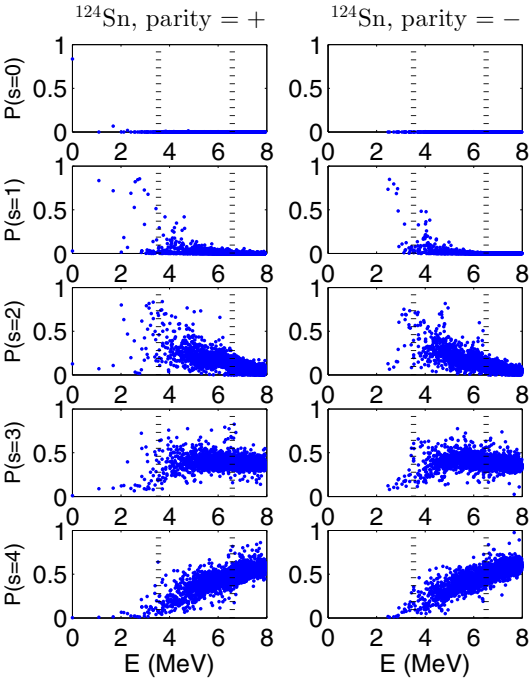

FIG. 21. Amplitudes of each generalized seniority versus the excitation energy in ^{124}Sn.

We also notice that in Figs. 4–12 some data points have large $\bar{s}$ but small excitation energy E (lying toward the top-left corner). These states should be identified as collective states and deserve more attention.

Figures 4–12 show that in general the level density ρ in a logarithmic scale increases linearly with the excitation energy. However, the $\rho(E)$ curves have a dip around $E^{<}_{s=1}$, for positive parity in $^{108-112}$Sn and negative parity in $^{108-114}$Sn. This is another piece of evidence for the persisting superfluid structure; the $s = 1$ broken-pair states have close energies and this group is quite separated in energy from the group of $s = 2$ broken-pair states. The dips are more apparent for negative parity, which should be related to the role of the intruder orbit $0h_{11/2}$.

The level densities up to the neutron separation energy in ^{116,118,122}Sn have been extracted experimentally under certain assumptions [27–29]. However the computed level densities of this work are smaller than the experimentally extracted ones near the neutron separation energy. The reasons are as follows. First, the adopted interaction [13] was fitted by only the first few low-lying states and may not be very accurate at higher energies. For example, the recently observed isomers of ^{124}Sn, 13^- and 15^-, were measured [14] at excitation energies $E(13^-) = 4324$ keV and $E(15^-) = 4553$ keV. The exact shell model with the adopted interaction [13] gives $E(13^-) = 4684$ keV and $E(15^-) = 4830$ keV. Second, we notice from Figs. 2 and 3 that systematically the generalized-seniority energies lie slightly higher than the exact ones. Third, at high energies the cross-shell excitations become important but these are missing in the current model space (the neutron 50–82 major shell). Therefore, the aim of this work is not to reproduce accurately the experimental level densities. Rather we investigate the generalized-seniority pattern generated by one of the most advanced modern realistic interactions [13].

Above we see evidence for the persisting superfluid structure. Meanwhile, sizable generalized-seniority mixing exists in all the $^{108-124}$Sn nuclei, even near the midshell. For $^{110-118}$Sn in Figs. 5–9, the stairs of the $\bar{s}$ staircase curves never sit at integers; the first and the second stairs are close to $\bar{s} = 1.5$ and 2.5, instead of 1 and 2. The fluctuation Δs (11) measures directly the degree of generalized-seniority mixing. In Figs. 4–12 Δs is sizable around 0.7 and decreases slightly with increasing excitation energy. Whether the slight decrease was realistic, reflecting less generalized-seniority mixing, or just an artificial effect of the current calculation that restricts the model space to $|s = 4\}$ (four broken pairs) deserves further study. For ^{108}Sn in Fig. 4 and ^{124}Sn in Fig. 12, the slight decrease is realistic because our results are the exact shell-model ones. For other nuclei future calculations within larger model spaces ($s > 4$) are necessary. At a given excitation energy, the spread of Δs is rather small; hence nearby eigenstates have quite similar degrees of generalized-seniority mixing. Practically no pure ($\Delta s \approx 0$) generalized-seniority state exists; the only three exceptions are a positive-parity state (∼7.7 MeV) and a negative-parity one (∼ 9 MeV) in ^{108}Sn, and a negative-parity one in ^{124}Sn (∼7.7 MeV). All three states are at high excitation energies and appear in nuclei far from the midshell. The results suggest more care to schematic studies using pure generalized-seniority states. For

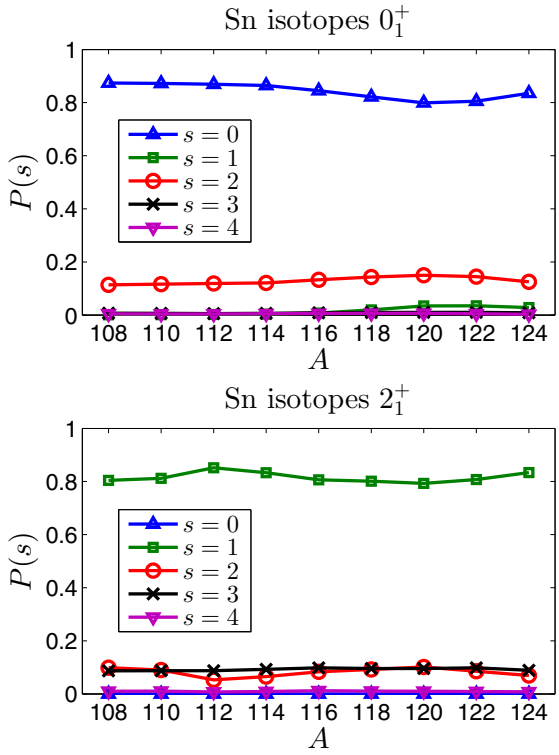

FIG. 22. Generalized-seniority compositions $P(s)$ of the 0_1^+ and 2_1^+ states in Sn isotopes.

example, Maheshwari and Jain [16] treated the isomer states 10^+, 13^-, and 15^- in $^{116\text{-}130}$Sn as pure generalized-seniority states with $S = 2$, 4, and 4, respectively. While the treatment was simple and inspiring, these isomer states in fact have mixed generalized-seniority based on the results of the current work. Similar comments apply to the work of Morales *et al.* [15] who treated the first 2^+ state as a pure $S = 2$ state.

Figures 4–12 show the generalized-seniority mean $\bar{s}$ (9) and fluctuation Δs (11) of each eigenstate. The precise composition of the eigenstates could be resolved by the generalized-seniority amplitudes $P(s)$ (8), as plotted in Figs. 13–21 for $^{108-124}$Sn. The pattern of successive breakup of the condensed pairs is evident and more pronounced near the midshell. In each nucleus, the $P(s = 0)$ amplitudes are for a single basis state (3). About 80% of this basis state distributes in the ground state (see also Fig. 22), and the leftover percent is scattered in many excited 0^+ states. The $P(s = 1)$ amplitudes mainly distribute below $E^<_{s=1}$, beyond which the drop is apparent. The $P(s = 2)$ amplitudes mostly distribute between $E^<_{s=1}$ and $E^<_{s=2}$. Below $E^<_{s=1}$ the $P(s = 2)$ amplitudes are small but not negligible, indicating sizable generalized-seniority mixing into the $s = 1$ eigenstates. The $P(s = 3)$ amplitudes increase with the excitation energy, but the trend is different for nuclei near and far from the midshell. Far from the midshell the $P(s = 3)$ amplitudes are already large beyond $E^<_{s=1}$ and do not increase obviously at $E^<_{s=2}$, whereas near the midshell the $P(s = 3)$ amplitudes show discontinuities at $E^<_{s=1}$ and $E^<_{s=2}$, indicating the persisting superfluid structure. The $P(s = 4)$ amplitudes are small and demonstrate the quality of the current calculation truncated to the subspace $|s = 4\}$. If generalized seniority is a good truncation scheme, the $P(s)$ amplitudes should decrease with increasing s after the eigen wave function achieves convergence. Indeed this is the case here. The $P(s = 4)$ amplitudes are small, especially so for low-lying states and for nuclei around the midshell. [The $P(s = 4)$ amplitudes are not small for ^{108}Sn and ^{124}Sn, but the results of these two nuclei are the exact shell-model ones without truncation.] For $^{112-118}$Sn, the $P(s = 4)$ amplitudes are negligible below $E^<_{s=1}$ and tiny below $E^<_{s=2}$, announcing excellent convergence. No exception exists, therefore we should not miss any shell-model eigenstate. The tiny $P(s = 4)$ amplitudes suggest that around the midshell the superfluid structure persists the best and the generalized-seniority truncation is very effective, whereas these nuclei have the largest dimension in the standard shell model and are the most time-consuming.

Summarizing Figs. 13–21, in general the picture of successive breakup of condensed pairs is evident and more pronounced near the midshell owing to the enhanced pairing. At $E^<_{s=1}$ the drop of $P(s = 1)$ and the increase of $P(s = 2)$ are apparent, indicating the breakup of the second pair. Near the midshell, around $E^<_{s=2}$ the drop of $P(s = 2)$ and the increase of $P(s = 3)$ are also evident, revealing the breakup of the third pair. The superfluid structure dominates the low-lying spectrum and interprets the wave functions. Meanwhile, sizable generalized-seniority mixing exists and the eigenstates do not have pure generalized seniority. Figures 4–12 and Figs. 13–21 display the eigen wave functions from different aspects, and they together depict the generalized-seniority pattern.

The near constancy of the first 2^+ excitation energy has attracted lots of discussion. In fact, it led Talmi [18,19] to propose the generalized seniority as a good quantum number of the Hamiltonian. Talmi assumed the pair structure v_α (2) to be invariant along the tin isotopic chain and studied under what restrictions the $s = 0$ state and the $s = 1, J^P = 2^+$ state are eigen states of the Hamiltonian. The derived restrictions lead naturally the constant first 2^+ excitation energy in the chain. However, the adopted realistic interaction of this work does not fulfill Talmi's picture strictly. In Fig. 1 the pair structures v_j are not constant but vary moderately along the chain. Figure 22 shows the generalized-seniority composition $P(s)$ of the ground state 0_1^+ and the first excited state 2_1^+. These two states are not pure $s = 0$ and $s = 1$ states, but have appreciable generalized-seniority mixing. In the ground state 0_1^+ the dominate $s = 0$ component has amplitude $P(s = 0) \approx 0.85$, the secondary $s = 2$ components have amplitude $P(s = 2) \approx 0.13$, and other s components are very small. In the first excited state 2_1^+ the dominate $s = 1$ components have amplitude $P(s = 1) \approx 0.82$. Secondarily, the $s = 2$ and the $s = 3$ components are approximately of equal importance with amplitudes $P(s = 2) \approx 0.08$ and $P(s = 3) \approx 0.09$. The $P(s = 0)$ amplitude vanishes by symmetry and the $P(s = 4)$ amplitude is negligible. Although appreciable generalized-seniority mixing exits, we notice that the $P(s)$ compositions of the 0_1^+ and 2_1^+ states are almost invariant along the isotopic chain; its origin and possible connection to the constant 2^+ excitation energy deserve further study.

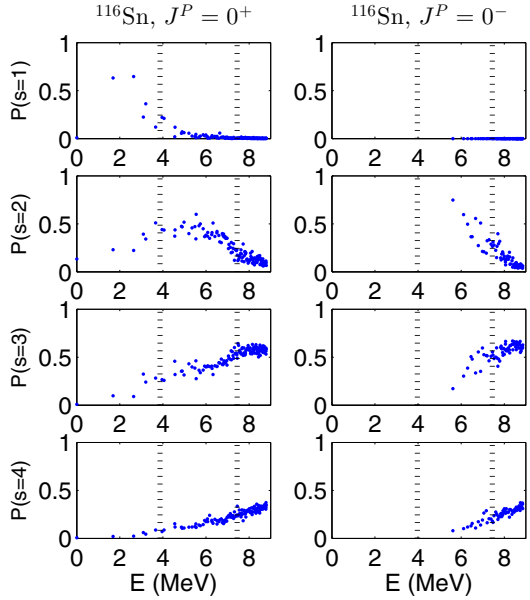

FIG. 23. Generalized-seniority amplitudes $P(s)$ of the $J = 0$ states in ^{116}Sn. In other words we take the data points from those in Fig. (17) corresponding to $J = 0$. The two vertical dotted lines $E = E^{<}_{s=1}$ and $E = E^{<}_{s=2}$ are at the same positions as those in Figs. 8 and 17.

Figures 4–21 distinguish the eigenstates only by parity due to the space limitation. More detailed information results from analyzing the eigenstates with the same angular momentum. Here we show eight examples of $J^P = 0^+, 0^-, 4^+, 4^-, 7^+, 7^-, 10^+, 10^-$ for the midshell nucleus ^{116}Sn in Figs. 23–26. We see that the $P(s)$ curve of a given J^P is much narrower (less dispersive at a specific excitation energy) compared with the $P(s)$ curve of a given parity P from Fig. 17. The shapes of the

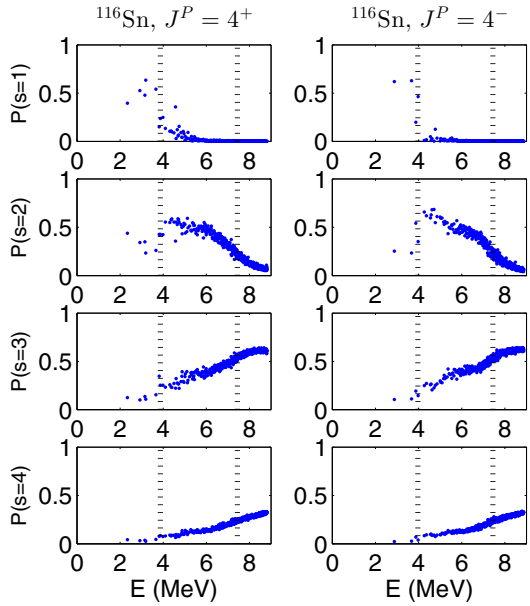

FIG. 24. Generalized-seniority amplitudes of the $J = 4$ states in ^{116}Sn.

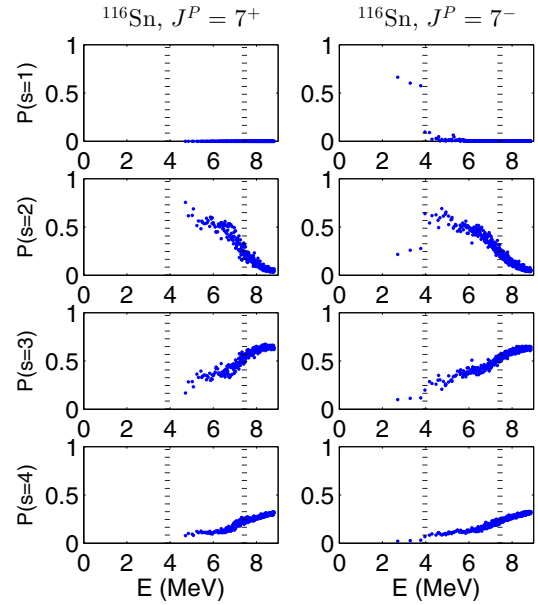

FIG. 25. Generalized-seniority amplitudes of the $J = 7$ states in ^{116}Sn.

$J = 0, J = 4, J = 7$, and $J = 10$ curves are different; higher J has sharper transitions. This suggests that the geometry of angular-momentum coupling plays an important role. The various J curves of different shapes overlap on Fig. 17 and result in a more dispersive $P(s)$ curve. Figures 23–26 show that between $E^{<}_{s=1}$ and $E^{<}_{s=2}$ the $P(s = 4)$ amplitudes are smaller for higher J, indicating better convergence. (The omitted figures of other J show the same trend.) Therefore the generalized-seniority approximation seems better for states of higher J, and this deserves further study.

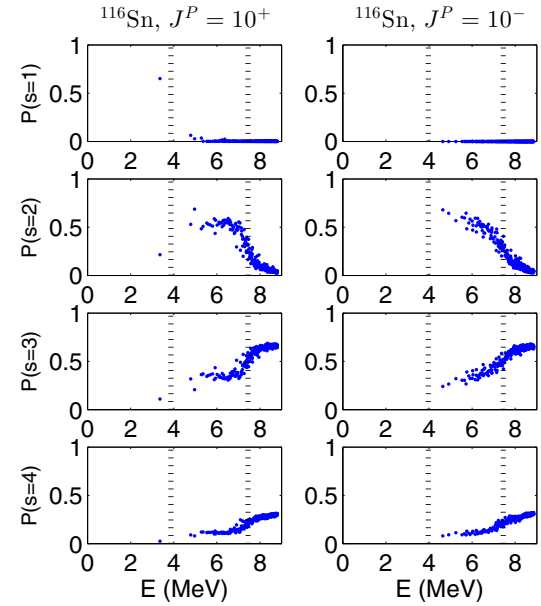

FIG. 26. Generalized-seniority amplitudes of the $J = 10$ states in ^{116}Sn.

IV. CANONICAL ENSEMBLE

In this section we compute the mean energy, entropy, and specific heat in the canonical ensemble. Defining $\beta \equiv 1/(k_B T)$, the partition function is

$$Z(\beta) = \sum_i e^{-\beta E_i} = \sum_J (2J+1) e^{-\beta E_J}. \tag{13}$$

The probability of occupying the many-body state i is

$$P_i = \frac{e^{-\beta E_i}}{Z}.$$

The mean energy, mean squared energy, and energy fluctuation are computed as

$$\langle E \rangle = \sum_i E_i P_i, \tag{14}$$

$$\langle E^2 \rangle = \sum_i (E_i)^2 P_i,$$

$$(\Delta E)^2 = \langle E^2 \rangle - \langle E \rangle^2. \tag{15}$$

The entropy and heat capacity are computed as

$$S = k_B \beta \langle E \rangle + k_B \ln Z.$$

$$C = k_B \beta^2 (\Delta E)^2.$$

For accuracy, we compute quantities by discrete summation rather than taking derivatives of the partition function.

Shell-model-type approaches apply two truncations in computing canonical-ensemble quantities: truncating the single-particle basis to the valence space, and the Lanczos diagonalization finds many-body eigenstates up to an energy cutoff, E_c. In this work the single-particle valence space is the neutron 50–82 major shell. This misses the cross-shell excitations at high excitation energies (around 8 MeV). The error owing to the Lanczos cutoff E_c is relatively easy to control; we vary E_c and the low-energy part of the results independent of E_c should be reliable.

We show the results of the canonical-ensemble mean-energy, entropy, and specific heat for three nuclei ^{108}Sn, ^{116}Sn, and ^{124}Sn in Figs. 27, 28, and 29. For each nucleus we take three cutoffs of $E_c = 8.5, 7.5$, and 6.5 MeV. [In Eqs. (13), (14), and (15) the summation includes eigenstates up to E_c.] The three corresponding curves below $k_B T = 0.5$ MeV overlap and should be reliable. The thermal pairing phase transition from the superfluid phase to the normal phase is reproduced.

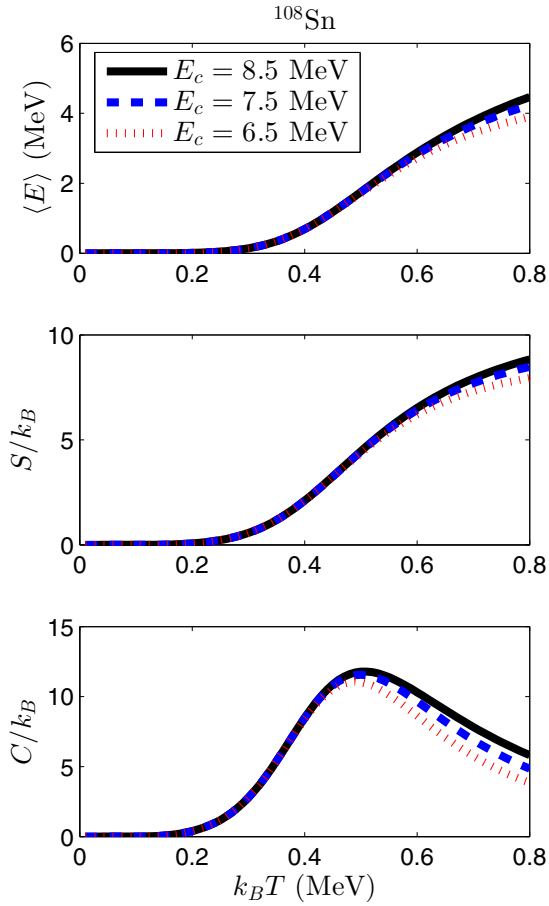

FIG. 27. The canonical-ensemble mean-energy $\langle E \rangle$, entropy S, and specific heat C versus the temperature T in ^{108}Sn. k_B is the Boltzmann constant. The three curves correspond to the three different energy cutoffs E_c.

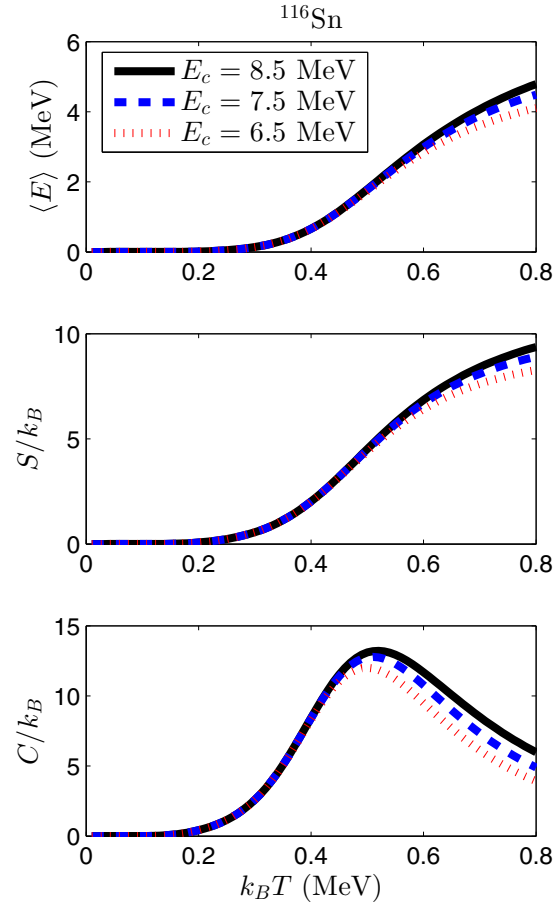

FIG. 28. The canonical-ensemble mean-energy, entropy, and specific heat versus the temperature in ^{116}Sn.

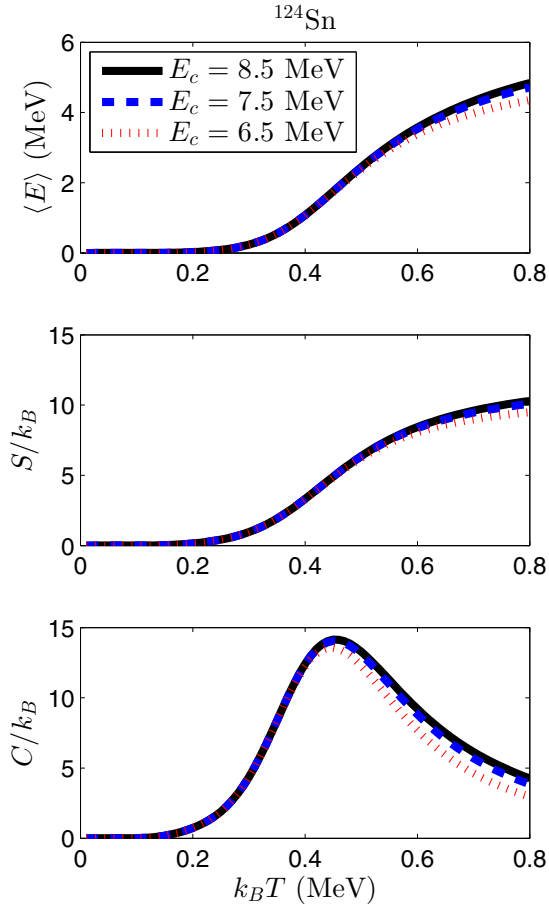

FIG. 29. The canonical-ensemble mean-energy, entropy, and specific heat versus the temperature in ^{124}Sn.

The steady decrease of the specific heat beyond $k_BT = 0.6$ MeV is unrealistic; the cross-shell excitations not included in the current model space (neutron 50–82 major shell) should become important.

V. CONCLUSIONS

We study even tin isotopes of mass number $A = 108$–124 with modern realistic interactions in the generalized-seniority truncation of the shell model. Allowing as many as four broken pairs, we compute for each nucleus the lowest 5000 eigenstates of each parity—up to around 8 MeV in excitation energy. The eigen wave functions converge well, especially so for low-lying states and for nuclei around the midshell. This work promotes the generalized-seniority approximation from "a viable first approximation" [11] to an accurate tool of serious realistic calculations for semimagic nuclei.

The structures of the eigen wave functions are investigated in terms of generalized-seniority in detail. For each eigenstate we compute the generalized-seniority ($S = 2s$) amplitudes $P(s)$, mean $\bar{s}$, and fluctuation Δs. The pattern of successive breakup of the condensed pairs is evident and more pronounced near the midshell owing to the enhanced collective pairing. Around the midshell, the transition is apparent from one to two broken pairs and is identifiable from two to three broken pairs. The superfluid structure generated by the pairing force persists at higher energies in the increasingly dense spectrum. The number of eigenstates below the first transition is roughly the same as the dimension of the one-broken-pair subspace; no further dimension truncation is possible. Away from the midshell the superfluid structure is more easily disturbed by other correlations at higher energies, but is still useful in interpreting the eigen wave functions.

Meanwhile, sizable generalized-seniority mixing exists even in the midshell region and practically no pure generalized-seniority state exists. This suggests more care when using pure generalized-seniority states to describe, for example, the seniority isomers. In particular, the near constancy of the first 2_1^+ excitation energy may not originate from a generalized-seniority conserving Hamiltonian. However, we observe that the generalized-seniority compositions $P(s)$ of the ground state 0_1^+ and the first excited state 2_1^+ are almost invariant along the isotopic chain (see Fig. 22); its origin and possible connection to the constant 2^+ excitation energy deserve further study.

We also calculate in the canonical ensemble the mean energy, entropy, and specific heat, based on the J-level spectrum up to high excitation energy. Computing this spectrum is feasible because of the much smaller dimension of the generalized-seniority truncated subspace compared with that of the standard shell model. The thermal pairing phase transition from the superfluid phase to the normal phase is reproduced.

ACKNOWLEDGMENTS

This work is supported by the National Natural Science Foundation of China under Grant No. 11405109, the Swedish Research Council (VR) under Grants No. 621-2012-3805 and No. 621-2013-4323, the Göran Gustafsson Foundation, and the Shanghai Key Lab of Modern Optical Systems. The shell-model calculations were performed on resources provided by the Swedish National Infrastructure for Computing (SNIC) at PDC at KTH, Stockholm.

[1] A. Bohr, B. R. Mottelson, and D. Pines, Phys. Rev. **110**, 936 (1958).
[2] S. Belyaev, Mat. Fys. Medd. K. Dan. Vidensk. Selsk. **31**, 641 (1959).
[3] J. Bardeen, L. N. Cooper, and J. R. Schrieffer, Phys. Rev. **108**, 1175 (1957).
[4] K. Allaart, E. Boeker, G. Bonsignori, M. Savoia, and Y. K. Gambhir, Phys. Rep. **169**, 209 (1988).
[5] J. Terasaki, J. Engel, M. Bender, J. Dobaczewski, W. Nazarewicz, and M. Stoitsov, Phys. Rev. C **71**, 034310 (2005).
[6] H. Shimoyama and M. Matsuo, Phys. Rev. C **84**, 044317 (2011).

[7] M. Grasso, D. Lacroix, and A. Vitturi, Phys. Rev. C **85**, 034317 (2012).
[8] G. Potel, F. Barranco, F. Marini, A. Idini, E. Vigezzi, and R. A. Broglia, Phys. Rev. Lett. **107**, 092501 (2011); G. Potel, A. Idini, F. Barranco, E. Vigezzi, and R. A. Broglia, Phys. Rev. C **87**, 054321 (2013).
[9] T. Niksic, D. Vretenar, P. Finelli, and P. Ring, Phys. Rev. C **66**, 024306 (2002).
[10] J. J. Li, J. Margueron, W. H. Long, and N. Van Giai, Phys. Rev. C **92**, 014302 (2015).
[11] D. J. Dean and M. Hjorth-Jensen, Rev. Mod. Phys. **75**, 607 (2003).
[12] B. A. Brown, N. J. Stone, J. R. Stone, I. S. Towner, and M. Hjorth-Jensen, Phys. Rev. C **71**, 044317 (2005).
[13] C. Qi and Z. X. Xu, Phys. Rev. C **86**, 044323 (2012).
[14] L. W. Iskra, R. Broda, R. V. F. Janssens, J. Wrzesinski, B. Szpak, C. J. Chiara, M. P. Carpenter, B. Fornal, N. Hoteling, F. G. Kondev, W. Krolas, T. Lauritsen, T. Pawlat, D. Seweryniak, I. Stefanescu, W. B. Walters, and S. Zhu, Phys. Rev. C **89**, 044324 (2014).
[15] I. Morales, P. V. Isacker, and I. Talmi, Phys. Lett. B **703**, 606 (2011).
[16] B. Maheshwari and A. K. Jain, Phys. Lett. B **753**, 122 (2016).
[17] B. Maheshwari, A. K. Jain, and B. Singh, Nucl. Phys. A **952**, 62 (2016).
[18] I. Talmi, Nucl. Phys. A **172**, 1 (1971).
[19] I. Talmi, *Simple Models of Complex Nuclei: The Shell Model and Interacting Boson Model* (Harwood, Chur, Switzerland, 1993).
[20] P. L. Ottaviani and M. Savoia, Phys. Rev. **187**, 1306 (1969).
[21] Y. K. Gambhir, A. Rimini, and T. Weber, Phys. Rev. C **3**, 1965 (1971).
[22] G. Bonsignori, M. Savoia, K. Allaart, A. van Egmond, and G. Te Velde, Nucl. Phys. A **432**, 389 (1985).
[23] M. Hjorth-Jensen, T. T. S. Kuo, and E. Osnes, Phys. Rep. **261**, 125 (1995).
[24] N. Sandulescu, J. Blomqvist, T. Engeland, M. Hjorth-Jensen, A. Holt, R. J. Liotta, and E. Osnes, Phys. Rev. C **55**, 2708 (1997).
[25] L. Y. Jia, J. Phys. G: Nucl. Part. Phys. **42**, 115105 (2015).
[26] C. Qi, L. Y. Jia, and G. J. Fu, Phys. Rev. C **94**, 014312 (2016).
[27] U. Agvaanluvsan, A. C. Larsen, M. Guttormsen, R. Chankova, G. E. Mitchell, A. Schiller, S. Siem, and A. Voinov, Phys. Rev. C **79**, 014320 (2009).
[28] H. K. Toft, A. C. Larsen, U. Agvaanluvsan, A. Burger, M. Guttormsen, G. E. Mitchell, H. T. Nyhus, A. Schiller, S. Siem, N. U. H. Syed, and A. Voinov, Phys. Rev. C **81**, 064311 (2010).
[29] H. K. Toft, A. C. Larsen, A. Burger, M. Guttormsen, A. Gorgen, H. T. Nyhus, T. Renstrom, S. Siem, G. M. Tveten, and A. Voinov, Phys. Rev. C **83**, 044320 (2011).
[30] M. Sano and S. Yamasaki, Prog. Theor. Phys. **29**, 397 (1963).
[31] A. L. Goodman, Nucl. Phys. A **352**, 30 (1981).
[32] G. H. Lang, C. W. Johnson, S. E. Koonin, and W. E. Ormand, Phys. Rev. C **48**, 1518 (1993).
[33] Y. Alhassid, D. J. Dean, S. E. Koonin, G. Lang, and W. E. Ormand, Phys. Rev. Lett. **72**, 613 (1994).
[34] H. Nakada and Y. Alhassid, Phys. Rev. Lett. **79**, 2939 (1997).
[35] H. Nakada and Y. Alhassid, Phys. Lett. B **436**, 231 (1998).
[36] S. Liu and Y. Alhassid, Phys. Rev. Lett. **87**, 022501 (2001).
[37] Y. Alhassid, G. F. Bertsch, and L. Fang, Phys. Rev. C **68**, 044322 (2003).
[38] C. Ozen, K. Langanke, G. Martinez-Pinedo, and D. J. Dean, Phys. Rev. C **75**, 064307 (2007).
[39] Y. Alhassid, L. Fang, and H. Nakada, Phys. Rev. Lett. **101**, 082501 (2008).
[40] C. Ozen, Y. Alhassid, and H. Nakada, Phys. Rev. Lett. **110**, 042502 (2013).
[41] Y. Alhassid, M. Bonett-Matiz, S. Liu, and H. Nakada, Phys. Rev. C **92**, 024307 (2015).
[42] N. Shimizu, Y. Utsuno, Y. Futamura, T. Sakurai, T. Mizusaki, and T. Otsuka, Phys. Lett. B **753**, 13 (2016).
[43] Y. K. Gambhir, A. Rimini, and T. Weber, Phys. Rev. **188**, 1573 (1969).
[44] S. Shlomo and I. Talmi, Nucl. Phys. A **198**, 81 (1972).
[45] R. Machleidt, Phys. Rev. C **63**, 024001 (2001).
[46] T. Back, C. Qi, B. Cederwall, R. Liotta, F. Ghazi Moradi, A. Johnson, R. Wyss, and R. Wadsworth, Phys. Rev. C **87**, 031306 (2013).
[47] M. G. Procter, D. M. Cullen, M. J. Taylor *et al.*, Phys. Rev. C **87**, 014308 (2013).
[48] L. F. Jiao, Z. H. Sun, Z. X. Xu, F. R. Xu, and Chong Qi, Phys. Rev. C **90**, 024306 (2014).
[49] M. Doncel, T. Back, D. M. Cullen *et al.*, Phys. Rev. C **91**, 061304 (2015).
[50] A. Neacsu and M. Horoi, Phys. Rev. C **91**, 024309 (2015).
[51] M. Horoi and A. Neacsu, Phys. Rev. C **93**, 024308 (2016).
[52] I. Talmi, Phys. Rev. C **25**, 3189 (1982).
[53] L. Y. Jia, Phys. Rev. C **93**, 064307 (2016).
[54] A. Banu *et al.*, Phys. Rev. C **72**, 061305(R) (2005).
[55] C. Vaman *et al.*, Phys. Rev. Lett. **99**, 162501 (2007).
[56] A. Ekstrom *et al.*, Phys. Rev. Lett. **101**, 012502 (2008).
[57] A. Jungclaus *et al.*, Phys. Lett. B **695**, 110 (2011).